

Fatigue Life Prediction for Aircraft Engine Piston Via Different Temperature

Tao-Tao Cheng*, Xin-Tian Liu**, Miao Liu*** and Kai Jin*

Keywords : piston, thermo-mechanical coupling, quality loss, temperature field.

ABSTRACT

The finite element calculation method of the piston was investigated with the piston as the research object. The method of setting the boundary conditions of the piston temperature field is determined. Structural analysis software is utilized to conduct a numerical analysis of the temperature and stress fields of the piston. The quality loss model examines the correlation between temperature and piston quality loss. The research and analysis can provide a more in-depth understanding of the heat of the piston and provide an accurate theoretical basis for optimal design, such as reducing heat load and improving stress distribution. It can be used for failure analysis of aircraft engine pistons, etc. to enhance the reliability and longevity of aviation piston engines.

INTRODUCTION

The piston forms the combustion chamber with the cylinder liner and cylinder head, enduring high pressure to output power through the connecting rod and crankshaft. Pistons are subjected to thermal and mechanical loads that directly affect engine performance. Cyclic thermal and mechanical stresses affect the piston's fatigue life, while temperature changes impact material properties and lubricant condition (2005). The reliability of the piston is self-evident. As a long-life, high-reliability product, the piston carries out many reliability tests to spend a lot of workforce and material resources, which is difficult for a company to bear. In recent decades, the rapid development of computer technology has made it

Paper Received January, 2024. Revised June, 2024. Accepted July, 2024. Author for Correspondence: Xin Tian Liu. xintianster@gmail.com

*** Professor, Department of Mechanical Engineering, Shanghai University of Engineering Science, Shanghai, Shanghai 201620, China.*

****Lecturer, Department of Mechanical Engineering, Shanghai University of Engineering Science, Shanghai, Shanghai 201620, China.*

** Graduate Student, Department of Mechanical Engineering, Shanghai University of Engineering Science, Shanghai, Shanghai 201620, China.*

possible to perform more accurate virtual simulations of pistons using finite element techniques, also favored by manufacturers. It has become the goal of many developers to assess the reliability of pistons using minimal data (2022). Considering the actual service conditions of the piston, it is necessary to conduct a thermal analysis. The thermal analysis methods of pistons mainly include experimental and numerical analysis methods.

To solve the time-consuming problem of solving fuzzy control equations, the linear elastic fuzzy finite element method was introduced (2006). Xue et al. (2013). investigated that S-FEM can work well with triangular and tetrahedral background cells and elements. Mourão et al. (2022). propose a computational framework to integrate the impacts of grain size distribution and morphology into numerical computations using Crystal Plasticity Finite Element (CPFE) method. Zhu et al. (2018) studied the Experimental deformation and numerical finite element analysis (FEA) of a full-size leaf disk test with increased step stress overloading. Karabulut (2011) investigated that a free-piston engine can be stabilized in a closed thermodynamic cycle over a small range of temperatures. Gao et al. (2023) and others forecast the fatigue lifespan of composite materials used in wind turbine rotor blades subjected to random loads. Cerit (2011) investigated how changes in coating thickness and width affect temperature and stress distribution, and conducted a comparative analysis with uncoated pistons.

Studies on engine heat transfer have used more experimental tests combined with simulation. Based on the thermocouple temperature test method and exploring the effect of engine load, Rakopoulo et al. (2000) investigated the transient heat transfer in cylinder heads and exhaust manifolds during cyclic duty cycles. Robinson et al. (2001) studied the development of piston temperature field simulations from one-dimensional models to two- and three-dimensional models.

Given some engineering practices, the magnitude of loss resulting from deviations in quality characteristics from the target value varies. Shaibu et al. (2006) analyzed the shortcomings of Taguchi's quadratic loss function and proposed two types of

exponential loss functions. Li (2002), and Chen (2006) proposed the asymmetric linear loss function and its segmented version as an alternative to the quadratic loss function proposed by Taguchi, which may not be suitable for expressing linear loss. Li (2019) and Xie mass loss more accurate. By the wear law, Liu et al. (2020) modified the value loss function during service and explored the effect of different parameters on product quality loss. Conducting reliability tests, complex systems fail for a variety of reasons, making it difficult to identify specific causes of failure. Li (2018), and Chen (2006) studied the asymmetric mass loss function to determine the optimal process parameters. Qian et al. (2020) created a dynamic model for quality characteristics that utilizes linear degradation and random error to forecast the quality loss of highly reliable long-life products.

Piston life is related to the cylinder temperature, and the surface temperature is influenced by gas forces and random loads. The piston skirt, having a lower temperature with a significant gradient, experiences thermal stresses that can cause deformation. Pistons endure gas pressure, inertial forces, lateral thrust, friction, and thermal stresses, potentially leading to top surface deformation, cracking, perforation, pin cracking, and increased skirt wear. These factors impact the piston's fatigue life, thereby affecting engine reliability.

This article applies FEA software to compute the temperature field and thermal stress distribution for aeronautical engine pistons based on their thermal conditions. In conjunction with the mechanical load experienced by the piston during actual operation, the thermal load and mechanical load are jointly analyzed to derive the coupled stress and deformation results of the piston. The effect of temperature on quality loss is obtained indirectly by improving the mass loss based on deformation.

THERMAL-MECHANICAL COUPLING FINITE ELEMENT ANALYSIS OF PISTON

Considering the thermal effect, the thermo-elasticity theory is studied, and the thermodynamic coupling analysis is completed. The piston heating and cooling process is analyzed using steady-state and transient heat analysis to determine the extent of thermal effects on the piston.

Material properties of the piston

Due to the working environment of the piston, high demands are placed on its materials:

- (1) The piston should be sufficiently rigid and robust to transmit forces reliably.
- (2) Good thermal conductivity, resistance to high pressure, high temperature, and wear and tear.
- (3) Small mass and lightweight to minimize

reciprocal inertia forces.

Aluminum alloy material meets the above requirements.

A four-stroke, four-cylinder horizontally opposed, liquid-cooled cylinder head, air-cooled cylinder block, spark plug ignition, and aero-piston engine with exhaust gas turbocharger are studied. Some basic parameters are listed in Table 1.

Table 1. Specific data for the tank vehicle.

Parts	E	μ	ρ	λ_t	β_t	σ_p	σ_s
	GP		kg/m ³	w/m·°C	/°C	MPa	MPa
Piston	71	0.3	2700	152	20.96 × 10 ⁻⁶	268.	260.7

The FEA is conducted based on the specified material parameters and the selected eutectic Al-Si alloy. Table 2 represents the performance parameters of the piston material.

Table 2. Material parameters of piston.

Name	Reference value
Cylinder bore	79.5mm
Piston stroke	61mm
Compression ratio	9:1
Power	75kW
Rotational speed	5000r/min
Total mass of the piston	0.300kg
Maximum burst pressure	65MPa
Connecting rod length/crank radius ratio	0.2877
Number of cylinders	4
Total cylinder displacement	1.2L
Single cylinder displacement	0.3L
Length of valve top rod	106mm
Ignition sequence	1-4-2-3
Crank offset	0mm

Boundary conditions of the model

(1) Steady-state temperature field control equation

Assumptions: The object is a continuous homogeneous medium; the parameters vary continuously and can be differentially derived. According to the law of conservation of energy and Fourier's law, the differential equation of thermal conductivity is obtained:

$$\rho c \frac{\partial T}{\partial t} = \frac{\partial}{\partial x} \left(\lambda_x \frac{\partial T}{\partial x} \right) + \frac{\partial}{\partial y} \left(\lambda_y \frac{\partial T}{\partial y} \right) + \frac{\partial}{\partial z} \left(\lambda_z \frac{\partial T}{\partial z} \right) + \dot{q} \quad (1)$$

where \dot{q} is the internal heat source intensity, c is the specific heat capacity of the thermal conductor, ρ is the thermal conductor density, and $\lambda_x, \lambda_y, \lambda_z$ denote the thermal conductivity of the piston material in the x, y, z direction. The left end represents the increment of the thermodynamic energy of the microelement the sum of the three terms on the right end represents the net heat flux into the microelement.

Suppose that the thermal conductivity is a constant, then it can be simplified as:

$$\rho c \frac{\partial T}{\partial t} = \lambda_x \frac{\partial^2 T}{\partial x^2} + \lambda_y \frac{\partial^2 T}{\partial y^2} + \lambda_z \frac{\partial^2 T}{\partial z^2} + \dot{q} \quad (2)$$

where the thermal conductivity is a constant, steady state, simplifies to:

$$\lambda_x \frac{\partial^2 T}{\partial x^2} + \lambda_y \frac{\partial^2 T}{\partial y^2} + \lambda_z \frac{\partial^2 T}{\partial z^2} + \dot{q} = 0 \quad (3)$$

With constant thermal conductivity, no internal heat source, and a steady state, it simplifies to:

$$\frac{\partial^2 T}{\partial x^2} + \frac{\partial^2 T}{\partial y^2} + \frac{\partial^2 T}{\partial z^2} = 0 \quad (4)$$

(2) Thermal boundary conditions

Supposing the fluid is cooled:

$$q_w = \lambda_t (T_f - T_w) \quad (5)$$

where T_f and T_w denote the fluid temperature and wall temperature, respectively, λ_t is the thermal conductivity.

The common thermal boundary conditions can be divided into three categories.

(a) The first type is that the temperature on the boundary is given. The general case is the temperature function on the boundary of a known object, which can be expressed as:

$$T|_{\Gamma} = f(x, y, z, t) \quad (6)$$

where Γ is the object's boundary, the direction of Γ is counterclockwise; $f(x, y, z, t)$ is the known wall temperature function with position and time.

(b) The second type is that heat flow density on the boundary is given. Since the direction of q is the same with the normal n outside the boundary surface, it is expressed as:

$$\left. \begin{aligned} -\lambda_t \frac{\partial T}{\partial n} \Big|_{\Gamma} &= q_2 \\ -\lambda_t \frac{\partial T}{\partial n} \Big|_{\Gamma} &= g(x, y, z, t) \end{aligned} \right\} \quad (7)$$

where q_2 is heat flow density, and $g(x, y, z, t)$ is heat flow density function.

(c) The third type is where α and T_f are given, which can be expressed as:

$$-\lambda_t \frac{\partial T}{\partial n} \Big|_{\Gamma} = \alpha (T - T_f) \Big|_{\Gamma} \quad (8)$$

where α and T_f are often regarded as constants in numerical calculations. This equation applies to both the solid being heated and cooled.

The boundary for piston without an internal heat source belongs to the third category conditions. According the heat transfer coefficient, medium temperature and Laplace equation, it can be obtained:

$$J = \int_V \left\{ \frac{\lambda}{2} \left[\left(\frac{\partial T}{\partial x} \right)^2 + \left(\frac{\partial T}{\partial y} \right)^2 + \left(\frac{\partial T}{\partial z} \right)^2 \right] \right\} dx dy dz + \int_S \alpha (T^2 - T_f T) ds \quad (9)$$

The generic expression for the delineation unit is:

$$J_C = \int_{V_C} \left\{ \frac{\lambda}{2} \left[\left(\frac{\partial T}{\partial x} \right)^2 + \left(\frac{\partial T}{\partial y} \right)^2 + \left(\frac{\partial T}{\partial z} \right)^2 \right] \right\} dx dy dz + \int_{S_C} \alpha (T^2 - T_f T) ds \quad (10)$$

The generalized function takes the extreme value condition as:

$$\frac{\partial J}{\partial T_i} = \sum_C \frac{\partial J_C}{\partial T_i} = 0, i = (1, 2, 3, \dots, n) \quad (11)$$

where J_C is the portion of the cell that overlaps the overall boundary, n is the total number of nodes.

According to the variational principle and the general function extreme value solution, the structural

temperature function is solved by first discretizing the structure to create general function and temperature dependent expressions for each unit; then superimposing the expressions to get the overall structure and temperature expression; and determining the structural node temperature values using the general function extreme value solution.

1) Average heat transfer coefficient at the top of the piston

The three common boundary conditions for piston heat transfer are simply stated: The first type is determined by measuring the piston's surface temperature. The second type is determined by heat flux. The third category pertains to the correlation between the convective heat transfer coefficient and the ambient temperature.

According to the modified Eichelberg formula, the gas heat transfer coefficient α_g per degree of crankshaft angle is calculated as:

$$\alpha_g = k_0 \sqrt[3]{C_t \sqrt{P_g T_g}} \quad (12)$$

where k_0 is the correction coefficient, C_t is the average piston speed, T_g represents the instantaneous temperature of the gas in the cylinder. P_g represents the instantaneous pressure of the gas within the cylinder.

The average heat transfer coefficient in a working cycle can be obtained by integrating the mean value:

$$\alpha_{gm} = \frac{1}{4\pi} \int_0^{4\pi} \alpha_g d\theta \quad (13)$$

Similarly, the average gas temperature T_{gm} within a working cycle can be obtained.

2) Heat transfer coefficient at each position of the piston top surface

The heat transfer coefficient of the piston's top surface varies with the radial position, and can be expressed by the following formula for different positions:

Suppose $r < N$,

$$\alpha_r = \frac{2 \cdot \alpha_{gm}}{1 + e^{0.1 \left[\frac{N}{25.4} \right]^{1.5}}} e^{0.1 \left[\frac{r}{25.4} \right]^{1.5}} \quad (14)$$

Suppose $r > N$,

$$\alpha_r = \frac{2 \cdot \alpha_{gm}}{1 + e^{0.1 \left[\frac{N}{25.4} \right]^{1.5}}} e^{0.1 \left[\frac{2N-r}{25.4} \right]^{1.5}} \quad (15)$$

where α_{gm} represents the average heat transfer coefficient within the cylinder, r_t represents the radial distance from the piston's center. and N represents the distance from the center of the piston to the location of the maximum heat transfer coefficient.

Numerous studies have shown that the highest piston temperature and at the throat, and also this location is where the heat transfer coefficient is maximum. Eqs. (14) and (15) determine the heat transfer coefficients on the top of the piston at specific circumferential locations. To apply thermal boundary conditions more efficiently and accurately control the thermal performance of the model, the top surface area is divided into four regions. The partitioning being shown in Figure 1.

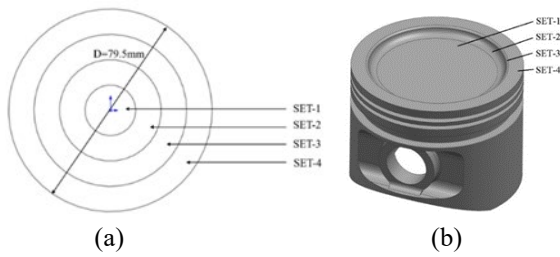


Fig. 1. Piston partition:(a) Partitioning of the piston top;(b) Geometric partitioning of piston

According to the distribution law of the local heat transfer coefficient, the top surface of the piston is divided into ring zones with intervals of approximately 10 mm. Given that the piston radius is 39.75 mm, divided into four rings, as follows:

$$\sum_{k=1}^4 S_k \alpha_k = S \alpha_{gm} \quad (16)$$

where S is the piston top area, S_k is the K -th ring area, and α_k is the K -th ring heat transfer coefficient.

According to the statistics of the study, from the center of the piston outwards as the radius increases, the heat transfer coefficient of each ring zone is reduced to 0.95 in the upper ring zone.

The top surface of the piston is divided into 4 ring zones, S_1 , S_2 , S_3 , and S_4 , from the innermost to the outermost layer.

$$\begin{aligned} S_1 &= 0.314 \times 10^{-3} m^2 \\ S_2 &= 0.942 \times 10^{-3} m^2 \\ S_3 &= 1.571 \times 10^{-3} m^2 \\ S_4 &= 2.199 \times 10^{-3} m^2 \end{aligned}$$

3) Heat transfer coefficient of piston ring groove and skirt

Ring groove area heat transfer coefficient:

$$\alpha_1 = \left(\frac{a}{\lambda_1} + \frac{b}{\lambda_2} + \frac{c}{\lambda_3} + \frac{1}{\lambda_\omega} \right)^{-1} \quad (17)$$

Skirt heat transfer coefficient:

$$\alpha_2 = \left(\frac{b}{\lambda_2} + \frac{b}{\lambda_3} + \frac{1}{\lambda_\omega} \right)^{-1} \quad (18)$$

Firepower shore heat transfer coefficient:

$$\alpha_3 = \left(\frac{\Delta n}{\lambda_1} + \frac{b}{\lambda_3} + \frac{1}{\lambda_\omega} \right)^{-1} \quad (19)$$

where λ_1 , λ_2 and λ_3 are the corresponding thermal conductivity of piston ring, oil film and cylinder liner respectively. a , b and c are the corresponding thickness of piston ring, oil film and cylinder liner respectively, λ_ω is the heat transfer coefficient between cylinder liner and cooling water, Δn is the gap between the cylinder liner and piston ring.

4) The heat transfer coefficient of the piston cavity is relatively stable, we can obtain:

$$\alpha_n = \frac{(T_1 - T_2) \cdot \lambda_t}{(T_2 - T_n) \cdot \delta} \quad (20)$$

where δ , T_1 are the thickness of the top of the piston, and the temperature, T_2 is the temperature at the bottom of the piston cavity, and T_n is the temperature inside the crank box.

Based on empirical equations, the heat transfer boundary conditions of the piston are predicted, and the critical point temperature of the surface is corrected through actual measurements. Data

regarding the variation of the piston surface heat transfer coefficient with ambient temperature were obtained. The current model lacks the capability for on-site testing of piston temperatures, thus preliminary calculations are conducted using empirical formulas. According to similar model's heat transfer boundary conditions, the final surface boundary conditions of the piston temperature field are presented in Table 3.

Table 3 Thermal boundary condition of piston.

position	Ambient temperature /°C	Heat transfer coefficient /W/m²·K
Piston top 1	1150	650
Piston top 2	1090	350
Piston top 3	1090	300
Piston top 4	1090	300
Fire shore	130	240
Upper first ring	220	2320
Middle of the first ring	220	1040
Lower first ring	220	2280
First ring bank	170	580
Upper second ring	160	2020
Middle of the second ring	160	2200
Lower second ring	160	1870
Second ring bank	160	1130
Upper third ring	140	2100
Middle of the third ring	140	1870
Lower third ring	140	1600
lumen	120	1000
Piston skirt	130	1000

Analysis of mechanical forces

The piston is subjected to gas pressure, inertial forces, and lateral tensile forces during engine operation, resulting in high stresses inside the piston known as mechanical stresses. The forces or torques include: F_G , generated by gas pressure at the piston crown in contact with the combustion chamber; F , generated by lateral pressure between the piston skirt and cylinder wall; M , the torque due to F relative to the piston pin axis; F_f , friction generated by piston reciprocating motion; M_f , torque due to F_f relative to the piston pin axis; F_{IC} , inertia force during piston reciprocating motion, adjustable to improve efficiency by modifying piston shape, size, and position; F_{IP} , inertia force on the piston pin primarily caused by piston reciprocating motion

This article mainly studies several forces which greatly influence the piston: gas pressure F_G , reciprocating inertia force F_{IC} and side pressure F of the piston skirt. The effect of other forces and torques is small. Fig. 2 shows the force borne by the piston

after simplification.

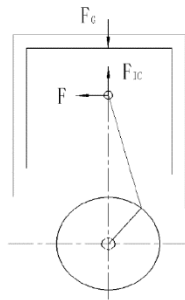


Fig. 2. Simplified diagram of piston forces

(1) Reciprocating inertia force of piston

The inertial force is expressed as mass times acceleration. The direction is opposite to its motion

$$a_j = -r_m \omega^2 (\cos \alpha + \mathfrak{R} \cos 2 \alpha_m) \quad (21)$$

The reciprocating inertia force can be calculated:

$$\bar{F} = -m \times a_j \quad (22)$$

where r_m is the radius of the crank, \mathfrak{R} is the ratio of connecting rods, ω is the angular speed of rotation of the crankshaft, α_m is the crank angle and m is the mass of the piston.

(2) Piston side thrust

There are two main reasons for the piston to generate side thrust: one is that under the action of high-temperature gas, the piston deforms due to temperature changes, resulting in side thrust when it contacts the cylinder liner; the other reason is that the piston, connected to the connecting rod via the piston pin, experiences the combined effects of high temperature, gas pressure, and inertia force during reciprocating motion, also causing side thrust.

(3) Skirt friction

Friction is usually generated in two ways, one during the reciprocating motion of the piston in the cylinder liner as a result of primary and secondary thrust. The other in the combined effect of thermal and mechanical loads, piston deformation will increase friction.

In a complete working cycle, the mechanical load suffered by the piston changes with time. Considering that the maximum burst pressure is the most significant mechanical load on the engine piston and that the reciprocating inertia forces are relatively small, calculating the lateral thrust is relatively difficult, and the frictional forces can be neglected under normal circumstances. The mechanical load boundary condition studied in this paper mainly refers to the maximum explosion pressure of the gas.

The establishment of piston solid model

The result of FEA is directly affected by meshing, poor meshing quality will lead to significant deviation of calculation results or can't run normally. To conduct a detailed analysis of the heat transfer coefficient on the piston crown, it is necessary to consider the characteristics of the heat transfer

coefficient variation with radius prior to grid partitioning. This will enable a more efficient setup of the heat transfer coefficient and thermal boundary conditions. The simulation process for the piston model is illustrated in Fig. 3.

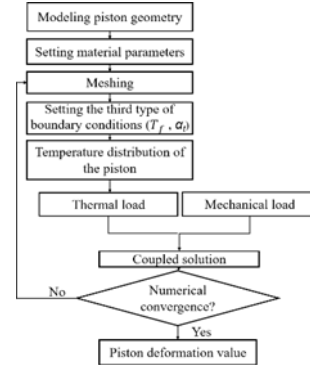


Fig. 3. Flowchart of piston model simulation.

During grid division, to enhance the operational efficiency of the analysis software and improve the quality of the grid, the piston model was simplified correctly without affecting the calculation results:

- 1) Neglecting the oil guide hole, and due to the chamfering of the piston ring area, the chamfer radius is very small and directly made into a right angle.
- 2) Simplify some irregular surfaces of the piston without compromising the accuracy of the calculations.

Five sets of piston mesh were constructed, named Mesh1, Mesh2, Mesh3, Mesh4, and Mesh5, corresponding to grid cell sizes of 0.006 m, 0.005 m, 0.004 m, 0.003 m, and 0.0025 m, respectively, to conduct the mesh sensitivity test. Fig.4 shows the grid partitioning model. The variation of simulation results with different mesh types is shown in Fig. 5, it can be seen that as the number of grids increases, the effect on the maximum deformation of the piston top becomes negligible after the number of grids reaches 270 753. Therefore, to ensure the accuracy and reduce the calculation volume, grid 4 with 270 753 grids is chosen as the reference.



Fig. 4. Piston mesh mode.

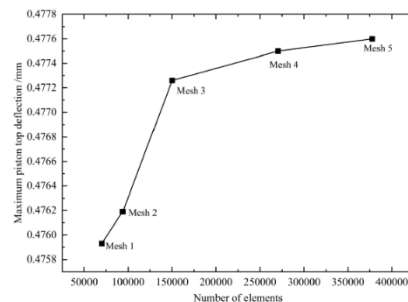


Fig.5. Variation of simulation results with different mesh types.

Analysis of piston temperature field results

The piston temperature field is divided into steady-state analysis and transient analysis. The steady-state temperature field is typically modelled using the finite element method. The transient temperature field describes the significant displacement of the piston’s top surface during engine operation, which increases its contact area with the cooling medium, inducing a thermal shock effect and elevating the temperature at the piston’s top. To investigate the relationship between deformation and temperature at the piston’s top, a transient temperature field model of the piston was developed.

The transient temperature field is calculated based on a simplified mesh model using the third type of boundary conditions piston thermal boundary conditions. Fig. 6 depicts the temperature distribution along the length of the piston and the inhomogeneity of the radial temperature at the top. The temperature at the top of the piston is significantly higher than that at the skirt, and the temperature decreases gradually from the top to the skirt along the length of the piston. The flow of cooling gas moves the local high temperature region from the combustion chamber wall to the centre, resulting in an overall temperature increase, especially at the exhaust side where the maximum temperature at the piston throat reaches 486.55°C. The temperature at the bottom and edges of the piston is relatively stable, with a minimum temperature of about 125.14°C, which is mainly concentrated at the lower part of the skirt. When the piston is located in the first ring groove, the temperature varies significantly, about 35°C. The high temperature zone is mainly located in the piston head.

As shown in Fig. 6, the deformation of the piston under the action of the coupling changes significantly: the deformation at the top is the most significant, reaching a maximum of 0.48 mm. The deformation of the inner cavity is very small and uniformly distributed. From the head to the skirt of the piston, the deformation gradually decreases. The inlet and exhaust valve groove structure of the pit on the upper surface of the piston and the asymmetric design of the inner cavity lead to the piston deformation not being completely symmetric along the centre axis of the piston during the coupling process.

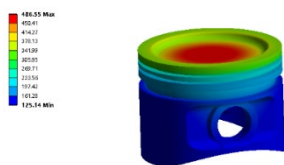


Fig. 6. Piston temperature distribution.

Improved quality loss model

Assuming that all other conditions remain constant, different temperatures are used to investigate the change in piston deformation with temperature.

Table 4 shows the deformation of the top piston surface at different temperatures. As depicted in Fig. 7, as the temperature increases, the deformation of the piston top surface increases, and the curve is similar to that of the tensile strength of the two metals as the temperature increases.

Table 4 Correspondence table of temperature and time relationship.

Temperature /°C	Deformation / mm
500	0.3531
600	0.3722
890	0.4660
1050	0.4775
500	0.3531
600	0.3722

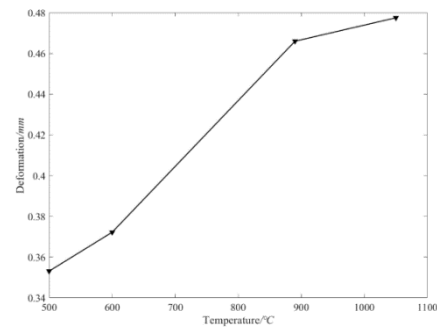


Fig. 7. Graph of temperature and deformation.

According to different temperatures and corresponding deformation amounts, the least square method can fit the curve equation of the deformation law. The amount of deformation is expressed by $H(T)$, and the temperature is expressed by T . It can be introduced into the variation law of operating environment parameters in the mass loss model.

Taguchi believed that the quality of a product cannot be solely determined by whether it meets the tolerance specifications. The Nominal-The-Best loss function can be represented by the following formula (Taguchi et al., 1989).

$$l(x) = k(x - m_q)^2 \tag{23}$$

where k represents the coefficient of quality loss during processing, $k = \frac{C_m}{\Delta^2}$.

The average quality loss of the product is expressed as follows:

$$E[l(x(t))] = k [\sigma_x^2 + (\mu_x - m_q)^2] \tag{24}$$

where μ_x represents the mean, σ_x represents the variance, $x(t)$ is considered as a random variable.

Considering the relationship between quality characteristics and time. After the product is put into use, the main quality characteristics of the product will gradually change with the growth of the working time of the mechanical parts. For many products, the values of quality characteristics during service vary linearly with time (Teran et al.,2021; Chen et al.,2019).

The variation of $\mu_x(t)$ and $\sigma_x(t)$ with the service time of the product as follows:

$$\begin{cases} \mu_x(t) = \mu_x(0) + \alpha t & t \geq 0 \\ \sigma_x(t) = \sigma_x(0) + \beta t & t \geq 0 \end{cases} \quad (25)$$

where $\mu_x(0)$ and $\sigma_x(0)$ represent the average and deviation from the mean of the product's quality characteristics at the time of departure from the factory, respectively. α , β is defined as service parameters.

The critical quality attributes of a product should demonstrate non-linear variations. By introducing $H(T)$, it is obtained as follows:

$$\begin{cases} \mu_x(t) = \mu_x(0) + H(T)t & t \geq 0 \\ \sigma_x(t) = \sigma_x(0) + \beta t & t \geq 0 \end{cases} \quad (26)$$

Eq. (26) should capture the pattern of product failure changes, which should closely resemble the pattern observed in practical applications, particularly in terms of deformation.

Supposed that the quality characteristics of the product follow a normal distribution before the product is put into service, denoted as $x(0) \sim N(\mu_x(0), \sigma_x^2(0))$, the mean and variance will change as the service life increases. At time t , the quality characteristics of the product also follow a normal distribution, denoted as $x(t) \sim N(\mu_x(t), \sigma_x^2(t))$. Suppose that $\alpha > 0$, $\alpha < 0$ and $\beta \geq 0$, then $\mu_x(t)$ decreases with the extension of the service life, while $\sigma_x^2(t)$ increases with the extension of the service life. As a result, the probability distribution density function $f(x(t))$ becomes flatter and flatter over time, indicating a broader spread of values. Additionally, the peak of $f(x(t))$ may shift to the left or right, reflecting the change in the mean $\mu_x(t)$. These changes signify the impact of the product's usage on its quality characteristics. During the repairable stage of the product, the quality characteristics of the product reach the upper and lower limits of the Preventive maintenance (PM). This information is depicted in Fig. 8. In the figure $t_3 > t_2 > t_1 = 0$. Specifically, t_3 indicates the time required for preventive replacement in case the minimum cost threshold is exceeded.

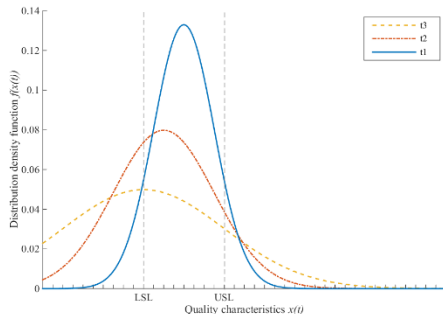


Fig. 8. Change diagram of quality characteristic distribution.

The quality characteristics $x(0)$ will obey a truncated normal distribution whose probability density function can be expressed as follows:

$$f(x(0)) =$$

$$\begin{cases} \frac{1}{(F(x_{USL}) - F(x_{LSL}))\sqrt{2\pi}\sigma_x(0)} e^{-\frac{(x(0) - \mu_x(0))^2}{2(\sigma_x(0))^2}} & x_{LSL} \leq x(0) \leq x_{USL} \\ 0 & \text{else} \end{cases} \quad (27)$$

where x_{USL} is the upper limit of the technical standard for quality characteristics, x_{LSL} is the lower limit. $F(x_{USL}) = \Phi\left(\frac{x_{USL} - \mu_x(0)}{\sigma_x(0)}\right)$, $F(x_{LSL}) = \Phi\left(\frac{x_{LSL} - \mu_x(0)}{\sigma_x(0)}\right)$, $x_{LSL} = m - \Delta$, $x_{USL} = m + \Delta$, and $x_{LSL} \leq x(0) \leq x_{USL}$.

The mean $\mu_x(t)$ and variance $\sigma_x(t)$ of the critical quality characteristic will change over time, $x_{LSL} \leq x(t) \leq x_{USL}$. $x(t)$ should also follow a truncated normal distribution whose probability density function can be expressed as follows:

$$f(x(t)) = \begin{cases} \frac{1}{(F(x_{USL}) - F(x_{LSL}))\sqrt{2\pi}(\sigma_x(0) + \beta t)} e^{-\frac{(x(t) - \mu_x(t))^2}{2(\sigma_x(0) + \beta t)^2}} & x_{LSL} \leq x(t) \leq x_{USL} \\ 0 & \text{else} \end{cases} \quad (28)$$

Based on the previous analysis, if the quality characteristic value exceeds the specified range $[x_{LSL}, x_{USL}]$, the probability of the product requiring repair from the start of its service until time t can be determined as follows:

$$P(t) = \int_{x_{LSL}}^{x_{USL}} \{f[x(0)] - f[x(t)]\} dx \quad (29)$$

By derivation of the above formula, the density function of the distribution of the product's service life, which is determined by the tolerance requirements of the desired quality characteristics, can be expressed as:

$$\xi(t) = \frac{dP(T < t)}{dt} = 0.4 \times \left[\left(\frac{\alpha}{\beta t + \sigma_x(0)} - \frac{\beta(\mu_x(t) - x_{USL})}{(\beta t + \sigma_x(0))^2} \right) \times e^{-\frac{(\mu_x(t) - x_{USL})^2}{2(\beta t + \sigma_x(0))^2}} - \left(\frac{\alpha}{\beta t + \sigma_x(0)} - \frac{\beta(\mu_x(t) - x_{LSL})}{(\beta t + \sigma_x(0))^2} \right) \times e^{-\frac{(\mu_x(t) - x_{LSL})^2}{2(\beta t + \sigma_x(0))^2}} \right] \quad (30)$$

After a product is delivered, a specific quality characteristic x initially conforms to specifications but changes randomly over time. At time t , this characteristic may exceed technical requirements, leading to product obsolescence. Assuming non-conformance results in a cost Cm , the present value of quality loss due to deviation from the target value after leaving the factory is recorded as $L(t)$. As the product continues in use, its quality characteristics keep changing, eventually resulting in obsolescence at time t with a loss of Cm . The cash flow calculation proceeds as follow (Peng et al., 2008):

$$C_m = L(t)(1 + r)^t \quad (31)$$

The loss in quality resulting from product scrapping is discounted using the following method:

$$L(t) = C_m(1 + r)^{-t} \quad (32)$$

where the annual interest rate is denoted by r . $[0, Cm]$ to express the range of present values of product quality losses.

The life cycle of a product is subject to random variations and a quality loss model can be developed using the probability density function of the product life distribution. Assuming that time is measured in hours, each hour is divided into m time intervals, with the total number of time intervals being tm . The duration of each time interval is dt , denoting the incremental time unit. The loss incurred in each time

interval is given by multiplying C_m by $\zeta(t)$ and dt , where $\zeta(t)$ denotes the probability density function of the product life distribution. The present value of product quality losses can be calculated using the following equation:

$$\begin{aligned} dL(t) &= \lim_{m \rightarrow +\infty} C_m \zeta(t) dt \left(1 + \frac{r}{m}\right)^{-tm} \\ &= C_m \zeta(t) dt \lim_{m \rightarrow +\infty} \left(1 + \frac{r}{m}\right)^{-tm} \\ &= C_m \zeta(t) \exp(-rt) dt \end{aligned} \quad (33)$$

The average quality loss of products within the service life T is shown as follows:

$$L_{LC} = C_m \int_0^T \zeta(t) \exp(-rt) dt \quad (34)$$

The quality loss model, which considers the wear regularity of a product and is based on its distribution density function of service life, can be established by substituting Eq. (30) into Eq. (34):

$$\begin{aligned} L_{LC} &= 0.4 \times C_m \int_0^T \left[\left(\frac{\alpha}{(\beta t + \sigma_x(0))} - \frac{\beta(\mu_x(t) - x_{USL})}{(\beta t + \sigma_x(0))^2} \right) \times e^{-\frac{(\mu_x(t) - x_{USL})^2}{2(\beta t + \sigma_x(0))^2}} \right. \\ &\quad \left. - \left(\frac{\alpha}{(\beta t + \sigma_x(0))} - \frac{\beta(\mu_x(t) - x_{LSL})}{(\beta t + \sigma_x(0))^2} \right) \times e^{-\frac{(\mu_x(t) - x_{LSL})^2}{2(\beta t + \sigma_x(0))^2}} \right] \exp(-rt) dt \end{aligned} \quad (35)$$

CASE STUDY

As depicted in Fig. 9, there is a maximum allowable space limit between the engine's piston and cylinder liner. Mutual wear between these components increases the clearance over time, leading to performance degradation. In the design process, it is assumed that there is no wear of the cylinder liner, and the clearance is primarily caused by piston wear. The piston dimensions and tolerances are $\Phi 50.8_{-0.01}^{+0.01}$, $\Delta = 0.01$, $m_x = 50.8$, $x_{USL} = 50.81$, $x_{LSL} = 50.79$. Assume that the machine is machining a batch of pistons with normally distributed outer diameters, the average dimension is $\mu_x(0) = 50.8$, and the mean variance is $\sigma_x(0) = 0.0033$. The cost of scrapping a piston is taken as $C_m = 150$, while $\beta = 0.00045/y$, $r = 10\%$, $\alpha = -0.0015/y$.

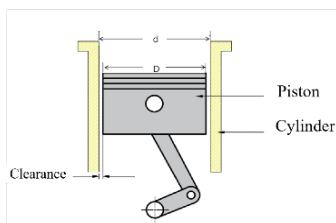


Fig. 9. A piston-cylinder bore assembly.

where D represents the diameter of the piston, d represents the distance between the cylinder liners.

The relationship between piston and service life was obtained through numerical calculation, as shown in Fig. 10. From Fig. 10, the service life of the product is approximately 812 hours. According to Fig. 11, the quality loss of the pistons in this batch starts to increase considerably between 0 and 500 hours, until after 3000 hours, the average quality loss of the pistons no longer increases and stabilizes at a constant value.

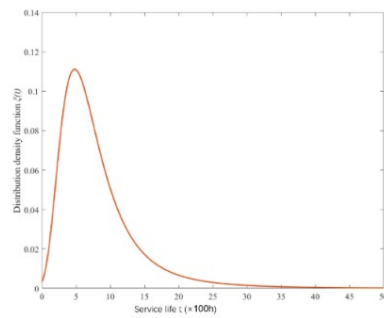


Fig. 10. Plot of piston life probability distribution density versus change in service life.

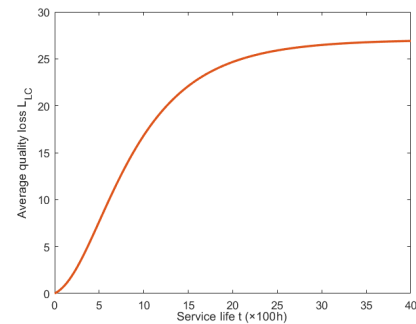


Fig. 11. Plot of average piston quality loss versus change in service life

CONCLUSIONS

Temperature can change the stability of the piston, reduce the material mass and affect the mechanical properties of the piston. It is necessary to investigate the mechanism of temperature on the mass and mechanical properties of the piston. The results are as follows:

(1) The effects of the piston temperature field, thermal and mechanical coupling stress on piston deformation are analyzed. The maximum piston deformation is up to 0.48 mm, and with the increase in temperature, this number will show a trend of increase.

(2) The influence of the deformation on the quality loss and service life of the piston is calculated by combining the piston deformation and the product service life density function, and the influence of temperature on the quality loss and service life of the piston is obtained indirectly.

ACKNOWLEDGMENT

This work is supported by Ministry of Science and Technology, Science and Technology Innovation 2030 New Generation Artificial Intelligence Major Project (2020AAA0109300), and the 2023 Young Scholars Cultivation fund in School of Mechanical and Automotive Engineering.

REFERENCES

- Cerit, M., “Thermo mechanical analysis of a partially ceramic coated piston used in an SI engine,” *Surf Coat Tech.*, Vol.205, No.11, pp.3499-3505 (2011).
- Chen, C.H., “Determining the optimum process mean for a mixed quality loss function,” *Int J Adv Manuf Tech.*, Vol.28, pp.571-576 (2006).
- Chen, C.H., and Chou, C.Y., “Determining the Optimum Process Parameters by Asymmetric Quality Loss Function,” *Matematika.*, Vol.22, No.2 (2006).
- Gao, J.X., Heng, F., and Yuan, Y.P., “Fatigue reliability analysis of composite material considering the growth of effective stress and critical stiffness,” *Aerospace.*, Vol.10, No.9, pp.785 (2023).
- Jiang, Z.M., Xu, W.Y., and Zhang, X.M., “Fast Solution of the governing equations of fuzzy finite element method on elastic media,” *Engineering Mechanics.*, Vol.23, No.7, pp.25-30 (2006).
- Kim, D.H., and Kim, B., “Estimation of die service life for a die cooling method in a hot forging process,” *Int J Adv Manuf Tech.*, Vol.27, pp.33-39 (2005).
- Karabulut, H., “Dynamic analysis of a free piston Stirling engine working with closed and open thermodynamic cycles,” *Renew Energ.*, Vol.36, No.6, pp.1704-1709 (2011).
- Li, M.H.C., “Unbalanced Tolerance Design and Manufacturing Setting with Asymmetrical Linear Loss Function,” *Int J Adv Manuf Tech.*, Vol.20, No.5, pp.334-340 (2002).
- Li, S.S., Liu, X.T., and Wang, Y.S., “A cubic quality loss function and its applications,” *Qual Reliab Eng Int.*, Vol.35, No.4, pp.1161-1179 (2019).
- Liu, X.T., Mao, K., and Wang, X.L., “A modified quality loss model of service life prediction for products via wear regularity,” *Reliab Eng Syst Safe.*, Vol. 204, pp.107187 (2020).
- Li, S.S., Liu, X.T., and Wang, Y.S., “Hidden quality cost function of a product based on the cubic approximation of the Taylor expansion,” *Int J Prod Res.*, Vol.56, No.14, pp.4762-4780 (2018).
- Li, Y., Zhang, X.G., and Ran, Y., “Early failure modeling and analysis of CNC machine tools,” *Int J Adv Manuf Tech.*, Vol.112, No.9-10, pp.2731-2754 (2021).
- Mourão, A., Correia, J., and Sun, J., “Computational investigation of Várzeas bridge steel under monotonic tensile via crystal plasticity finite element method,” *Procedia Struct.*, Vol.42, pp.1744-1751 (2022).
- Pan, X., Liu, J., and Li, Y., “A study on modified P-S-N curve of notched specimens based on small sample under multiaxial loading,” *Fatigue Fract Eng M.*, Vol.45, No.12, pp.3577-3591 (2022).
- Peng, H. P., Jiang, X. Q., and Xu, Z. G., “Optimal tolerance design for products with correlated characteristics by considering the present worth of quality loss,” *The International Journal of Advanced Manufacturing Technology*, Vol.39, pp.1-8 (2008).
- Qian, K.F., Liu, X.T., and Mao, K., “Quality loss prediction of mechanical system life considering linear degeneration and random error,” *Qual Reliab Eng.*, Vol.37, No.3, pp.935-949 (2020).
- Rakopoulos, C.D., Mavropoulos, G.C., and Hountalas, D.T., “Measurements and analysis of load and speed effects on the instantaneous wall heat fluxes in a direct injection air-cooled diesel engine,” *Int J Energ Res.*, Vol.24, No.7, pp.587-604 (2000).
- Robinson, D., and Palaninathan, R., “Thermal analysis of piston casting using 3-D finite element method,” *Finite Elem Anal Des.*, Vol.37, No.2, pp.85-95 (2001).
- Shaibu, A.B., and Cho, B.R., “Development of realistic quality loss functions for industrial applications,” *J Syst Sci and Syst Eng.*, Vol.15, No.4, pp.385-398 (2006).
- Taguchi, G., Elsayed, E.A., and Hsiang, T.C., *Quality Engineering in Production Systems*, McGraw-Hill International Editions, Singapore (1989).
- Teran, A., Pratted, B., and Case, K.E., “Present worth of external quality losses for symmetric nominal-is-better quality characteristics,” *Eng Econ.*, Vol.42, No.1, pp.39-52 (1996).
- Xue, B.Y., Wu, S.C., and Zhang, W.H., “A smoothed FEM (S-FEM) for heat transfer problems,” *Int J Comp Meth.*, Vol.10, No.01, pp.1340001 (2013).
- Xie, W., “Optimal pricing and two-dimensional warranty policies for a new product,” *Int J Prod Re.*, Vol.55, No.22, pp.6857-6870 (2017).
- Zhu, S. P, Liu, Q., and Peng, W., “Computational-experimental approaches for fatigue reliability assessment of turbine bladed disks,” *Int J Mech Sci.*, Vol.142, pp.502-517 (2018).
- Zhao, Y., Liu, D., and Zeng, L., “Modeling present worth of product quality losses based on service life distribution,” *Chin J Mech Eng-en.*, Vol.48, No.20, pp.182-191 (2012).

NOMENCLATURE

Parameter names	Parameter Description	Unit
θ	Crankshaft angle	rad
α_g	Heat flow density	W/m ² -K
α_{gm}	Average heat transfer coefficient	W/m ² -K
α_1	Heat transfer coefficient of	W/m ² -K

	the ring groove area	
α_2	Heat transfer coefficient of the skirt heat	$W/m^2 \cdot K$
α_3	Heat transfer coefficient of the firepower shore	$W/m^2 \cdot K$
α_n	Heat transfer coefficient of the piston cavity	$W/m^2 \cdot K$
T_f	Fluid temperature	$^{\circ}C$
T_w	Wall temperature	$^{\circ}C$
T_g	Instantaneous temperature of the gas in the cylinder	$^{\circ}C$
T_{gm}	Average gas temperature	$^{\circ}C$
T_1	Piston top temperature	$^{\circ}C$
T_2	Temperature at the bottom of the piston chamber	$^{\circ}C$
T_n	Inside the crank box temperature	$^{\circ}C$
λ_t	Thermal conductivity of the piston material	$W/m \cdot ^{\circ}C$
λ_1	Thermal conductivity of piston ring	$W/m \cdot ^{\circ}C$
λ_2	Thermal conductivity of oil film	$W/m \cdot ^{\circ}C$
λ_3	Thermal conductivity of cylinder liner	$W/m \cdot ^{\circ}C$
λ_{ω}	Heat transfer coefficient between cylinder liner and cooling water	$W/m \cdot ^{\circ}C$
λ_x	Thermal conductivity of piston in x-direction	$W/m \cdot ^{\circ}C$
λ_y	Thermal conductivity of piston in y-direction	$W/m \cdot ^{\circ}C$
λ_z	Thermal conductivity of	$W/m \cdot ^{\circ}C$
k_0	Correction coefficient	
Γ	Boundary	
F	Side pressure	N
F_f	Friction	N
\bar{F}	Inertia force	N
F_{IC}	Piston inertia force	N
F_{IP}	Inertia force of piston pin	N
F_G	Gas pressure	Pa
M_f	Friction torque on the centerline of the piston pin	$N \cdot m$
M	Torque on the centerline of the piston pin	$N \cdot m$
\mathfrak{R}	Connecting rod ratio	
r	interest rate	%
α, β	service parameters	y (year)
k	Quality loss coefficient	
C_m	Present value of quality losses	

型來研究溫度變化與活塞隨時間變化的質量損失之間的關係。結果有助於優化活塞設計，提高航空發動機的可靠性和使用壽命。

不同溫度下航空發動機活 塞的疲勞壽命預測

程桃桃 劉新田 劉焱 靳凱
上海工程技術大學機械與汽車工程學院

摘要

該研究探討了航空發動機活塞的有限元分析 (FEA)，確定了設置活塞溫度場邊界條件的方法。通過使用結構分析軟件，進行了數值模擬，以評估活塞的溫度和應力分佈。以此為基礎用質量損失模